Influence of SO_3 on the MnO_x/TiO_2 SCR catalyst for elemental mercury removal and the function of Fe modification

Shibo Zhang [a], Qingzhu Zhang [a,*], Mercedes Díaz-Somoano [b], Juan Dang [a], Yang Xu [a], Yongchun Zhao [c,*], Junying Zhang [c]

[a] Environment Research Institute, Shandong University, Qingdao 266237, China.

[b] Instituto Nacional del Carbón (CSIC), Francisco Pintado Fe, 26, 33011 Oviedo, Spain.

[c] State Key Laboratory of Coal Combustion, School of Energy and Power Engineering, Huazhong University of Science and Technology, Wuhan 430074, China.

[*] Corresponding authors.

E-mail addresses: zqz@sdu.edu.cn (Q. Zhang), yczhao@hust.edu.cn (Y. Zhao).

Abstract

Elemental mercury (Hg^0) is a highly hazardous pollutant of coal combustion. The low-temperature SCR catalyst of MnO_x/TiO_2 can efficiently remove Hg^0 in coal-burning flue gas. Considering its sulfur sensitivity, the effect of SO_3 on the catalytic efficiency of MnO_x/TiO_2 and Fe modified MnO_x/TiO_2 for Hg^0 removal was investigated comprehensively for the first time. Characterizations of Hg-TPD and XPS were conducted to explore the catalytic mechanisms of Hg^0 removal processes under different conditions. Hg^0 removal efficiency of MnO_x/TiO_2 was inhibited irreversibly from 92% to approximately 60% with the addition of 50 ppm SO_3 at 150 ℃, which resulted from the transformation of Mn^{4+} and chemisorbed oxygen to $MnSO_4$. The existence of H_2O would intensify the inhibitory effect. The inhibition almost

disappeared and even converted to promotion as the temperature increased to 250 ℃ and above. Fe modification on MnO_x/TiO_2 improved the Hg^0 removal performance in the presence of SO_3. The addition of SO_3 caused only a slight inhibition of 1.9% on Hg^0 removal efficiency of Fe modified MnO_x/TiO_2 in simulated coal-fired flue gas, and the efficiency maintained good stability during a 12h experimental period. This work would be conducive to the future application of MnO_x/TiO_2 for synergistic Hg^0 removal.

Keywords: SO_3; MnO_x/TiO_2; Mercury; Fe modification; Mechanism

1. Introduction

Mercury (Hg) is a highly hazardous pollutant to ecological environment and human's health because of its acute toxicity, volatility and bioaccumulation (Obrist et al., 2017). Coal combustion is one of the major artificial mercury discharge sources. It accounts for almost a quarter of the total mercury emissions (UNEP, 2019). As the Minamata Convention came into force in 2017, a rigorous control on mercury emission from coal burning is an essential measure based on the dual pressure of environmental protection and convention fulfillment.

Among different existing types of mercury in coal combustion flue gas, elemental mercury (Hg^0) is volatile and insoluble (Yang et al., 2021), which makes it the most difficult Hg species to be removed. It is the crux for the mercury emission control. Using SCR (Selective Catalytic Reduction) catalyst which is installed for removing NO from coal-fired flue gas to synergistically convert Hg^0 to soluble oxidized mercury (Hg^{2+}), followed by Hg^{2+} being captured by wet flue gas desulfurization, has drawn

extensive attentions in recent years (Fernández-Miranda et al., 2016; Masoomi et al., 2020; Li et al., 2021). Compared to other approaches such as sorbent injection, this method utilizes the existing devices of coal combustion power plant to implement Hg^0 removal, with no need of extra equipment or reagents. Thus, the SCR catalytic oxidation can obviously save the cost for Hg emission control and reduce the risk of the secondary mercury pollution (Li et al., 2017), exhibiting distinct advantages and broad application prospects.

According to our previous research, manganese oxide supported on titanium (MnO_x/TiO_2) catalyst exerts prominent NO and synergistic Hg^0 removal activity at the working temperature of 200-250 ℃ which is lower than that of the commercial vanadium-based SCR catalyst (Zhang et al., 2017a). The remarkable low-temperature activity of MnO_x/TiO_2 makes it feasible to move the catalyst to more downstream position in the flue gas, even after the electrostatic precipitator (ESP), so as to mitigate the corrosion from fly ash (Wu et al., 2007). Then the defects of the commercial SCR catalyst will be eluded, which is beneficial to the catalytic performance and life span of the catalyst (Benson et al., 2005; Li et al., 2007). MnO_x/TiO_2 exhibits favorable Hg^0 removal activity in the low temperature range, however, the catalytic efficiency is apparently inhibited in the presence of SO_2. The Hg^0 oxidation efficiency decreased by almost 40% with the addition of 400 ppm SO_2 into the flue gas (Zhang et al., 2017a, 2017b). The formation of sulfate on the catalyst was confirmed to be the main reason for the inhibition. Hence, the poor sulfur resistance is the bottleneck of MnO_x/TiO_2 for commercial application in spite of its significant low-temperature activity.

It is quite worthwhile to notice that there is also a certain amount of SO_3 in coal-fired flue gas besides SO_2. SO_3 that will involve in the Hg^0 oxidation over SCR catalyst derives mainly from coal-S conversion during the combustion process and SO_2 oxidation by the SCR catalyst (Yang et al., 2018b; Lu et al., 2019). If the catalyst is placed in the lower reach of ESP, the injected SO_3 using for improving ESP performance should be considered as well (Presto and Granite, 2007). The concentration of SO_3 in actual flue gas is up to approximately 40 ppm (Tan et al., 2006; Zhou et al., 2019). Relative researches have been made to study the effects of SO_3 on the Hg removal activity of solid adsorbents. On one hand, compared with SO_2, SO_3 has a higher acid dew point and stronger reaction activity. As a result, SO_3 is much easier than SO_2 to condense on catalyst surface and transform to sulfate at low temperatures, thereby generating more serious inhibition on the catalytic efficiency, especially with the assistance of water vapor (H_2O). Presto et al. (2007) studied the effect of SO_3 on Hg capture by activated carbon and found that the Hg removal capacity declined as SO_3 concentration raised from 20 ppm to 100 ppm. The formation of hexavalent sulfur on the carbon surface was verified to be responsible for the inhibition. Krishnakumar et al. (2011) revealed that Hg removal by activated carbon was unaffected by less than 10 ppm of added SO_3, while it was restrained with the SO_3 concentration reaching 35 ppm. Sjostrom et al. (2009) prepared several bromine-treated and alkali-treated coal-based activated carbons and obtained that SO_3 would cause different levels of suppression on the Hg capture over the sorbents. He et al. (2012) demonstrated the inhibition of SO_3 on Hg adsorption on the graphene carbonaceous surface using quantum chemistry

method. On the other hand, SO_3 has stronger oxidation capacity than the lattice oxygen of SCR catalyst. It can oxidize Hg^0 to Hg^{2+}, which reveals a tendency to facilitate the Hg^0 oxidation performance. Investigation of Zhou et al. (2019) on the role of SO_3 in Hg^0 removal by magnetic biochar showed that Hg^0 oxidation efficiency of the sorbent was promoted by SO_3 because of the generation of more C=O functional groups on the sorbent surface. Yang et al. (2019) researched Hg^0 capture property of mineral sulfide, and the results indicated that Hg^0 could be oxidized by SO_3 to form $HgSO_4$ and immobilized on the nanosized CuS material. Zhang et al. (2020a) similarly confirmed that SO_3 could expedite the Hg^0 oxidation over a Cu/ZSM-5 molecular sieve catalyst through converting Hg^0 to $HgSO_4$, and the promotion was more distinct at higher temperature. Based on the existing researches, the influence of SO_3 on the heterogeneous oxidation of mercury is ambiguous, which depends on the specific type of catalyst or adsorbent and also probably the working conditions. Up to now, most of the existing studies on Hg^0 oxidation by SCR catalyst concerned the effects of the flue gas components of HCl, SO_2, NO and NH_3 but neglected SO_3. Moreover, some literatures that have considered the factor of SO_3 mostly focused on its influence on Hg^0 removal over adsorbent such as activated carbon and magnetic biochar. Few literatures have explored the role of SO_3 in Hg^0 oxidation performance of SCR catalyst systematically, especially the low-temperature SCR catalyst of MnO_x/TiO_2. Considering the low sulfur resistance of MnO_x/TiO_2, comprehending the effect of SO_3 on the Hg^0 removal is highly requisite for evaluation on the practical application prospect of this low-temperature SCR catalyst. In addition, Fe modification was

confirmed to be conducive to improving the resistance of MnO_x/TiO_2 to the SO_2 poisoning in our previous research. Hg^0 removal efficiency over the catalyst increased by 20.6% and 15.4% in the individual SO_2 component and simulated coal-fired flue gas (SFG) containing SO_2 respectively after Fe modification (Zhang et al., 2018). Nevertheless, the function of Fe modification to the effects of SO_3 on Hg^0 removal performance of the MnO_x/TiO_2 catalyst is currently unclear.

In this study, the effects of SO_3 on the Hg^0 adsorption and oxidation efficiencies of MnO_x/TiO_2 were comprehensively investigated under different reaction temperatures and water vapor concentrations by the continuous and transient experiments. Hg^0 removal efficiency of the Fe modified MnO_x/TiO_2 (Fe-MnO_x/TiO_2) catalyst was evaluated in the presence of SO_3 and H_2O as well and made comparisons with that of MnO_x/TiO_2 to examine the Fe modification effects. Other components in coal-fired flue gas, such as HCl, NO and NH_3, were not contained in the reaction gas in order to focus on the effect of SO_3 on Hg^0 removal exclusively and eliminate interference of these components. Nevertheless, experiments on Hg^0 removal over the catalysts were carried out in simulated coal combustion flue gas with full flue gas components including SO_3 to predict the catalytic activity and stability under actual working condition. Hg-TPD and XPS analysis methods were utilized to explore the influence mechanism of SO_3 on the Hg^0 removal performance and the corresponding mechanism of Fe modification on the effect of SO_3. This work will be highly conducive to further understanding the application potential of the MnO_x/TiO_2 catalyst in synergistic Hg^0 removal from coal combustion flue gas.

2. Materials and methods

2.1. Preparation and physical characterization of catalysts

The MnO_x/TiO_2 and Fe-MnO_x/TiO_2 catalysts employed in this work were prepared by a sol-gel method, and the preparation process has been described in our previous study (Zhang et al., 2017b, 2018). Briefly, the reagents of tetrabutyl titanate, manganese nitrate and ferric nitrate were selected as the precursors of the elements Ti, Mn and Fe in the catalysts. The precursor solutions were mixed and stirred for several hours at room temperature until the formed sol turned to gel. The gel then underwent the procedures of drying at 100 ℃ for 12 h, calcinating at 500 ℃ for 5 h, grinding and sieving with 200 mesh sequentially. The powder catalysts were finally obtained. The molar ratios of Mn/Ti and Fe/Ti in the catalysts were controlled at 0.8 and 0.2, respectively, which were determined to be the optimal ratios for the catalytic activity (Zhang et al., 2017a, 2018). The MnO_x/TiO_2 catalyst was demonstrated to exhibit superior mercury removal activity compared to commercial SCR catalyst, with the comparison results shown in Fig. S1 (Zhang et al., 2017b, 2020b). MnO_x/TiO_2 and Fe-MnO_x/TiO_2 are abbreviated as MnTi and FeMnTi, respectively, in the following sections.

The characterization methods of Hg-temperature programmed desorption (Hg-TPD) and X-ray photoelectron spectroscopy (XPS) were carried out over the fresh and spent catalysts to explain the experimental results and study related mechanisms. Hg-TPD was conducted from 20 ℃ to 800 ℃ at a heating rate of 10 ℃/min in 1 L/min N_2 over the catalysts, which were spent in the Hg^0 removal experiments in different

153 atmospheres. XPS was implemented on a PerkinElmer PHI 5100 ESCA system
154 operating at 8×10^{-10} Torr with an Al Kα X-Ray source (hν=1486.6eV) and passing
155 energy of 35.75eV, and the C 1s binding energy value of 284.6 eV was used for the
156 spectra calibration. The Brunauer-Emmett-Teller (BET) surface and X-ray diffraction
157 (XRD) analyses have been conducted previously for understanding the physico-
158 chemical properties of the catalysts. The results were shown in Table. S1 and Fig. S2,
159 respectively. The BET surface area of MnTi was 122.63 m^2/g, and it further increased
160 to 127.26 m^2/g after Fe modification. Both the surface areas were apparently higher
161 than that of commercial SCR catalyst (<100 m^2/g). The pore volume and size were
162 declined with Fe modification, which was perhaps due to the partial occupation of
163 surface micropores by the loaded Fe. Only weak characteristic peak of MnO_x was
164 observed on the XRD pattern of MnTi. The MnO_x peaks disappeared and no peaks
165 corresponding to FeO_x emerged on the pattern of FeMnTi. Fe modification improved
166 the dispersity of MnO_x and FeO_x on the catalyst surface. The large surface area and
167 well-dispersed metal oxides were beneficial for the catalytic activity. The BET and
168 XRD results indicated the synergistic effect of Fe and Mn in the catalyst.

169 *2.2. Catalytic activity measurement*

170 A bench-scale experimental system was employed for the experiments of this work,
171 as shown in Fig. 1. The individual flue gas components all came from cylinder gases,
172 and their flow rates were controlled accurately by the corresponding calibrated mass
173 flowmeters. Continuous feed of Hg^0 vapor was generated from a Hg^0 penetration tube
174 which was put in a U-tube and heated with a water bath, and the Hg^0 vapor was brought

into the flue gas by N_2. The initial Hg^0 concentration was kept at 70 μg/m^3 by controlling the temperature of water bath. SO_3 was produced by SO_2 oxidation by O_2 over a vanadium-titanium oxide based catalyst (VTBC) placed in a fixed-bed reactor. SO_2 oxidation efficiency was maintained at 100% via regulating the dosage of VTBC and the reaction temperature. It was affirmed by the non-detected SO_2 concentration at the outlet of the reactor with a gas analyzer (AFRISO, Multilyzer STe, M60), which indicated SO_2 was all converted to SO_3. As the O_2 concentration at percentage level was much higher than that of SO_2, the consumption of O_2 in the SO_2 oxidation was negligible. And the concentration of SO_3 in the flue gas was equal to and adjusted by the inlet concentration of SO_2. Water vapor was generated and introduced into the flue gas with a steam generator. The total gas flow was kept at 1 L/min. The catalytic reaction was proceeded in another temperature-controlled fixed-bed reactor. Hg^0 concentration in the flue gas was recorded continuously by an online mercury monitor (Ohio Lumex, RA-915M). The flue gas was washed by NaOH and silica gel before entering the monitor to eliminate the interferences of sulfur oxides and H_2O on the detecting results. An ion exchanger resin (Dowex 1×8) which was valid for selective extraction of Hg^{2+} species was used for determining the Hg^{2+} concentration at the outlet of the reactor. The pipeline of the system was heated with electric heating belt to avoid any possible condensations of the gas components before measurement. The exhaust gas was cleaned by active carbon before released to atmosphere.

In each test, the flue gas first passed through the bypass of the catalytic reactor to confirm the inlet Hg^0 concentration. Then the gas stream was switched to the reactor

loaded with catalyst sample until the monitored data reached stability, acquiring the outlet Hg^0 concentration. The catalyst dosage for each test was 50 mg unless otherwise stated. The stability was defined as the fluctuation of the data being no more than 5% for at least 30 min. The Hg^{2+} content in the resin after the test was measured by the mercury monitor coupled with a PYRO furnace to determine the outlet gaseous Hg^{2+} concentration. After each test of the experiment, fresh catalyst was replaced to start the next test. Each experiment conducted at the corresponding working condition was repeated for 3 times, and then averaged the results. The total Hg^0 removal efficiency (E_T), Hg^0 oxidation efficiency (E_{oxi}) and Hg^0 adsorption efficiency (E_{ads}) of the catalyst were investigated and calculated by Eqs. (1), (2) and (3), respectively.

$$E_T = \frac{Hg^0_{in} - Hg^0_{out}}{Hg^0_{in}} \times 100\% \quad (1)$$

$$E_{oxi} = \frac{Hg^{2+}_{out}}{Hg^0_{in} \cdot ft} \times 100\% \quad (2)$$

$$E_{ads} = E_T - E_{oxi} \quad (3)$$

In the equations, Hg^0_{in} and Hg^0_{out} represent the inlet and outlet gaseous Hg^0 concentrations, respectively. Hg^{2+}_{out} represents the Hg^{2+} content in the resin after each test. f and t are the gas flow and the duration time of the test, respectively.

3. Results and discussion

3.1. Effect of SO_3 on E_{ads}, E_{oxi} and E_T of MnTi

Effect of SO_3 on Hg^0 removal efficiency of the MnTi catalyst was first investigated at different temperatures, and the results were shown in Fig. 2. The SO_3 concentration was adjusted to 30, 50 and 80 ppm in the experiment which were in the same order of magnitude as its concentration in real flue gas. According to the results, Hg^0 adsorption

efficiencies were no more than 13.5% under all the conditions. The oxidation efficiencies accounted for the majority of the Hg^0 removal efficiencies. Thus, catalytic oxidation is the dominant Hg^0 removal process, which guaranteed the persistence of Hg^0 removal efficiency. The addition of SO_3 into the flue gas led to the decrease of E_{ads} at 100 ℃ and 150 ℃, which might be due to the generation of sulfite and sulfate on the catalyst surface, resulting in the reduced number of active sites and further the deactivation of the catalyst. Hg^0 oxidation over MnTi was proven to follow Mars-Maessen and Langmuir-Hinshelwood mechanisms in our previous studies (Zhang et al., 2017a, 2018). Specifically, Hg^0 adsorption is an essential procedure in the oxidation process, and the decline of Hg^0 adsorption capacity was accompanied by the drop of E_{oxi}. As a result, E_T of MnTi showed an obvious inhibition as SO_3 concentration increased from 0 to 80 ppm. The inhibitions of SO_3 on E_{ads}, E_{oxi} and E_T were all weakened with the rise in the temperature. The increased temperature was conducive to the decomposition of sulfite and sulfate, especially for sulfite, of which the pyrolysis temperature was lower than that of sulfate (Meng et al., 2019). Therefore, a portion of the active sites available for Hg^0 adsorption and oxidation was recovered under this condition, though high temperature was detrimental to Hg^0 adsorption. In addition, the energy barrier of the reaction of Hg^0 with SO_3 can be overcome at the higher temperatures. Then Hg^0 could be oxidized by SO_3 to generate $HgSO_4$ with the assistance of gaseous O_2 or chemisorbed oxygen (O_{ad}), as described by reaction (1) and (2) (Zhou et al., 2019; Li et al., 2011), which improved E_{oxi} of the catalyst. As a

$$Hg^0 + SO_3 + \frac{1}{2}O_2 \rightarrow HgSO_4 \quad (1)$$

$$Hg^0 + SO_3 + O_{ad} \rightarrow HgSO_4 \quad (2)$$

result, the inhibition of SO_3 on E_T almost disappeared as the temperature increased to 250 ℃. The variation trend of E_T converted to promotion with the augment of the SO_3 concentration when the temperature reached 300 ℃ and 350 ℃.

3.2. Co-effect of SO_3 and H_2O on E_{ads}, E_{oxi} and E_T of MnTi

Investigation on the effect of SO_3 on the catalytic performance of MnTi was made in the presence of H_2O as well considering the affinity between SO_3 and H_2O. As the results shown in Fig. 3, with the introduction of 10% H_2O into the flue gas of 4% O_2 + 80 ppm SO_3, E_{ads}, E_{oxi} and E_T of the catalyst were restrained at all the temperature points compared to those without adding H_2O, especially at the temperature of 100-200 ℃. SO_3 could react with H_2O to produce H_2SO_4 which was easier to condense on the catalyst, accelerating the conversion of metal active substances to corresponding sulfates. The active sites of the catalyst were thereby further reduced. As the temperature was lifted to 250 ℃ and above, Hg^0 could react with H_2SO_4 to generate $HgSO_4$ (Zhou et al., 2019; Uddin et al., 2008). $HgSO_4$ was difficult to decompose and would stably retain on the catalyst in the testing temperature range until adsorption saturation was reached (Rumayor et al., 2015a; Zhang et al., 2019). As a result, the inhibitory level of E_{ads} caused by the existence of H_2O was reduced, which was accordingly favorable for E_{oxi}. Furthermore, because of the simultaneous occurrence of the reaction of Hg^0 with SO_3, the inhibition of the co-effect of SO_3 and H_2O on E_{oxi} and E_T of the catalyst was alleviated obviously at 250-350 ℃. E_T was even superior in the copresence of SO_3 and H_2O to that under the condition of without SO_3 and H_2O at 300 ℃

and 350 ℃.

3.3. Function of Fe modification to the effects of SO_3 and H_2O on E_{ads}, E_{oxi} and E_T

Hg^0 removal efficiency of Fe modified MnO_x/TiO_2 catalyst was measured and made comparison with that of MnO_x/TiO_2 to understand the modification effect of Fe on the catalytic performance in the presence of SO_3 and H_2O. As the results shown in Fig. 4, Fe modification made an apparent improvement on E_{ads}, E_{oxi} and E_T of the catalyst in the flue gas with 50 ppm SO_3 added. The Fe modification could increase the number of active sites and the content of O_{ad} on the catalyst according to the results in our previous research (Zhang et al., 2018). Furthermore, Fe had a good affinity with the SO_4^{2-} ion to produce $Fe_2(SO_4)_3$. Hence, it provided a protection for the active Mn species to prevent them being converted to $MnSO_4$ by SO_3, and this speculation would be verified by the subsequent XPS analysis. Then Hg^0 adsorption quantity of the catalyst would be enhanced by the Fe modification. Correspondingly, E_{oxi} and E_T were incremented as well. E_{oxi} increased by 4.9%, 5.9%, 5.6%, 6.6%, 9.6% and 12.4%, respectively, at the six temperature points in the range of 100-350 ℃. The promotion of E_{oxi} became more evident as the temperature raised, which was attributed to the more O_{ad} generated from Fe modification facilitating Hg^0 oxidation through reaction (2) at higher temperature (Zhang et al., 2018; Li et al., 2011). It could be confirmed by the results of the subsequent Hg-TPD and XPS analyses that $HgSO_4$ was generated during the reaction in the presence of SO_3 at 250 ℃ while it was not generated at 150 ℃.

When H_2O was introduced into the SO_3-contained flue gas, the condensed H_2SO_4 on the catalyst enhanced the generation of sulfate which was difficult to pyrolyze. These

285 extra produced sulfates can further conjugate with Fe and Mn, leading to more severe
286 deactivation of the catalyst. Hence, the facilitation of Fe modification on E_{ads} was
287 reduced in the presence of H_2O. In addition, the existence of H_2O would hinder the
288 contact of gaseous Hg^0 and SO_3 with the surface active substances (Zhou et al., 2019).
289 Therefore, the promotion degree of E_{oxi} was also whittled at all the temperatures.
290 Considering the factors of E_{ads} and E_{oxi}, the promotional effect of the Fe modification
291 over E_T under the condition of SO_3 was weaker when exposed to H_2O than that in the
292 dry flue gas. Nevertheless, E_T of FeMnTi remained an enhancement of at least 5.2% in
293 the copresence of SO_3 and H_2O owing to the Fe modification.

294 *3.4. Transient effects of SO_3 and H_2O on E_T of MnTi and FeMnTi*

295 Transient response experiments were also carried out to understand the effects of
296 SO_3 and H_2O on Hg^0 removal efficiencies of the MnTi and FeMnTi catalysts, and the
297 results were shown in Fig. 5. As the experimental results depicted in Fig. 2-4, E_{ads}
298 occupied only a small percentage of E_T, while E_{oxi} made the major contribution to the
299 removal efficiency. Thus, it could be determined that E_T of the catalysts recorded
300 continuously by the efficiency curves were almost equivalent to E_{oxi} of the catalysts.
301 After E_T of the catalysts achieved stability in the atmosphere of N_2+4%O_2 at 150 ℃,
302 addition of 50 ppm SO_3 into the reaction gas generated an obvious inhibition on the
303 efficiency of MnTi, as the results shown in Fig. 5a. The efficiency decreased from 92%
304 to approximately 60%. If 50 ppm SO_3 and 10% H_2O were introduced at the same time,
305 E_T of MnTi declined to only 48%. After Fe modification, the efficiency of FeMnTi was
306 restrained by the addition of 50 ppm SO_3 and 10% H_2O as well. But the inhibitory extent

was weakened compared to that of MnTi in the same condition. Therefore, the results demonstrated the inhibition of SO_3 and H_2O on the Hg^0 removal performance and the modification effect of Fe on the resistance of the catalyst to SO_3 poisoning. As SO_3 and H_2O were switched off, E_T of MnTi and FeMnTi could not return to the original level, suggesting an irreversible inhibition. It further indicated that the catalyst venenation led by the formation of sulfite and sulfate was the primary reason for the inhibitory effect of SO_3 on the Hg^0 removal efficiencies. In the condition of injecting SO_3 solely, E_T of the catalysts was restored slightly after the addition of SO_3 was cut off. The possible explanation for this phenomenon was that the competitive adsorption was likewise the cause for the suppression besides the formation of sulfite and sulfate. The competitive adsorption between Hg^0 and SO_3 was also proven by the research of Zhuang et al. (2011) over activated carbon. Without SO_3 competing for the active sites with Hg^0, together with the easier Hg^0 adsorption at low temperature, the Hg^0 removal efficiency displayed a certain recovery as SO_3 was switched off. By contrast, E_T showed almost no recovery after the reaction in the flue gas with SO_3 and H_2O added simultaneously. The reasonable interpretation was that the existence of H_2O intensified the generation of sulfate on the catalysts, which would be evidenced by the follow-up XPS analysis as well. The active sites for Hg^0 adsorption were almost completely blocked by the generated sulfate, which led to a more drastic deactivation of the catalysts. Thus, E_T reflected little recovery as the introducing of SO_3 and H_2O was ceased.

With the temperature raised to 250 °C, there was a negligible variation on E_T of MnTi when SO_3 was added into the flue gas, as shown in Fig. 5b. This phenomenon

was probably due to the counteraction of the formation of sulfate and the Hg^0 oxidation by SO_3 at the higher temperature. Ascribing to the Fe modification bringing more O_{ad} for the catalyst and making protection on the active Mn species which has been confirmed by the XPS analysis in our previous study (Zhang et al., 2018), the addition of SO_3 led to a promotion on E_{oxi} and E_T of FeMnTi. Simultaneous addition of SO_3 and H_2O made the decrease of E_T over both MnTi and FeMnTi. Because of the enhancement on sulfur and H_2O resistance of the catalyst by Fe modification, the decline of E_T was relatively smaller over FeMnTi, and it was inhibited slightly by only about 4%. After the introduced gas was switched off, E_T of the four spent catalysts all revealed an apparent fall. On one hand, SO_3 could oxidize Hg^0 and promote E_{oxi} at 250 ℃. The promotion disappeared with the interruption of SO_3 supply, leading to the decrease of E_T. On the other hand, sulfite and sulfate were produced after the reaction in the presence of SO_3, which caused irreversible poisoning effect on the catalysts. And it was unfavorable for Hg^0 adsorption and oxidized by the catalysts at 250 ℃. This was another reason for the decrease of E_T. The removal efficiencies of the catalysts showed a larger decline after cutting off the transient reaction gas with H_2O, which likewise illustrated the acceleration of catalyst deactivation led by the coexistence of SO_3 and H_2O.

3.5. Effect of SO_3 on Hg^0 removal performance of MnTi and FeMnTi in SFG

In order to clarify the effect of SO_3 on Hg^0 removal performance of the catalysts under actual condition, E_T of MnTi and FeMnTi were detected in SFG (N_2 + 4%O_2 + 12%CO_2+400 ppm SO_2 + 400 ppm NO + 400 ppm NH_3 + 10 ppm HCl + 10%H_2O) plus

50 ppm SO_3, and the results were made comparison with those in SFG without SO_3. 0.5 g catalyst was used for this experiment. As the primary purpose of SCR catalyst is $deNO_x$, the experiment was conducted at 250 ℃ which was attested to be the optimal temperature for NO removal in the previous work (Zhang et al., 2017a, 2018). According to the acquired results shown in Fig. 6, E_T of MnTi showed a certain decrease as SO_3 was added into SFG, which was because SO_3 expedited the sulfating of active metal elements on catalyst surface. Nevertheless, perhaps due to the reasons such as the low SO_3 concentration, the pyrolysis of part sulfate at 250 ℃ and Hg^0 oxidation by SO_3, the decline of E_T was not dramatic (nearly 5.2%). After Fe modification, the inhibition of SO_3 on E_T in SFG was further alleviated. The addition of SO_3 led to only a slight decrease of 1.9% on E_T of FeMnTi. Meanwhile, E_T of the catalyst was improved apparently by the Fe modification in the simulated coal-fired flue gas. Similar to the results under SFG without SO_3, E_T of MnTi and FeMnTi in the presence of SO_3 maintained good stability during a relatively long experimental period of 12 h. The prominent catalytic sustainability is an important property for SCR catalyst since the catalyst is usually used for several years in power plant before replacement. Hence, it could be drawn that there were no evident influences on E_T of the catalysts under SFG with the addition of 50 ppm SO_3 which was close to the SO_3 concentration in actual flue gas. The catalysts could remain excellent Hg^0 removal performance in SFG with SO_3 existed, especially the Fe modified FeMnTi catalyst. As the temperature of 250 ℃ was obviously lower than the working temperature of commercial SCR catalyst (about 350-400 ℃) (Zhang et al., 2017a), the results indicated the remarkable low-temperature

activity of the catalysts for mercury removal in practical flue gas condition.

3.6. Characterization analysis on the MnTi and FeMnTi catalysts

3.6.1 Hg-TPD analysis

Characterization analyses over the fresh and spent catalyst samples were implemented in order to explore the influence mechanism of SO_3 on Hg^0 removal performance and the modification mechanism of Fe on the effect of SO_3. Hg-TPD analysis was carried out to identify Hg speciation on the catalysts. The blank experiment was first conducted over fresh MnTi and FeMnTi catalysts, with the results shown in Fig. S3. No mercury was detected from the fresh catalysts, indicating that the catalysts were free of mercury, and mercury detected on spent catalyst were all attributed to adsorbed Hg formed in the reaction. The catalysts after spent in different reaction gases were then analyzed, and the results were shown in Fig. 7. Hg adsorption contents on the spent catalysts were derived from the integral area of Hg-TPD profile, and the adsorption contents on unit mass of the catalysts were calculated and listed in Table 1. According to the results, Hg adsorption contents on MnTi were in the range of 0.806-1.858 μg/g. Relatively, the calculated values based on the catalytic efficiencies and reaction time of the continuous experiment with the results shown in Fig. 2 and 3 were 0.823-1.982 μg/g under the corresponding working conditions. The error range of the adsorption contents computed by the two approaches was no more than 6.3%. Therefore, the Hg species exhibited excellent mass balance in the reactions.

The Hg-TPD profiles of the catalysts after reacted at 150 ℃ were shown in Fig. 7a. A desorption peak corresponding to HgO and a weak peak assigning to physical

adsorbed Hg were observed at 471 ℃ and 165 ℃ respectively on the profile of MnTi after spent in N_2+4%O_2 (Rumayor et al., 2015b, 2017). The addition of 80ppm SO_3 into the reaction gas of N_2+4%O_2 led to the weakening of the HgO peak and the disappearance of the peak of physical adsorbed Hg. Hence, the existence of SO_3 at 150 ℃ impeded the Hg adsorption process on the catalyst surface, which was detrimental to E_{oxi} and E_T. A sequential injection of 10%H_2O led to a further attenuation of the peak intensity of HgO, suggesting H_2O intensified the inhibition of SO_3 on Hg^0 adsorption capacity of MnTi. After Fe modification, the HgO peak intensity was enhanced on the profile of FeMnTi compared to on that of MnTi after the catalysts were spent in the copresence of SO_3 and H_2O. Fe modification made the catalyst have more active sites available for Hg adsorption when exposed to the atmosphere of SO_3+H_2O. Hg^0 adsorption capacity of the catalyst was improved, and it was favorable to E_T under the condition.

As the reaction temperature increased to 250 ℃, the Hg-TPD profiles of the spent catalysts were shown in Fig. 7b. According to the results, the addition of SO_3 into N_2+O_2 resulted in the decrease of the desorption peak intensity of HgO on the profile of MnTi, which was similar to that at 150 ℃. Furthermore, a new peak corresponding to $HgSO_4$ emerged at 587 ℃ on the profile (Rumayor et al., 2015b), indicating that $HgSO_4$ was produced on the catalyst during the reaction in the presence of SO_3 at 250 ℃. SO_3 could facilitate Hg^0 oxidation to form $HgSO_4$ at higher temperature. This was one of the main reasons for the inhibition of SO_3 on E_T becoming weaker and even converting to promotion with the increase of temperature. Further addition of H_2O

417 engendered a more serious restriction on the peak intensity of HgO and Hg^0 adsorption
418 capacity of MnTi as well. The variation tendency of the Hg^0 adsorption capacity could
419 be identified more intuitively by the results presented in Table 1. Nonetheless, the peak
420 intensity of $HgSO_4$ was elevated compared to that before the injection of H_2O, which
421 demonstrated that the conversion of SO_3 to H_2SO_4 in the presence of H_2O promoted the
422 formation of $HgSO_4$ on the catalyst surface. It helped reduce the inhibition on E_{ads}
423 caused by the co-effect of SO_3 and H_2O as the temperature rose, which was beneficial
424 to E_{oxi} and E_T. Perhaps because $HgSO_4$ occupied part of the active sites, the
425 improvement of the HgO peak intensity and Hg adsorption content led by the Fe
426 modification at 250 ℃ was slighter than that at 150 ℃ in the copresence of SO_3 and
427 H_2O.

428 Based on the above results, the ordinal addition of SO_3 and H_2O into the flue gas
429 led to a gradual deepening inhibition on Hg^0 removal performance of MnTi. The
430 negative effect of SO_3 and H_2O on E_T was weakened with the increase of temperature
431 due to the generation of $HgSO_4$. Fe modification on MnTi could enhance the sulfur
432 resistance of the catalyst, bringing higher Hg adsorption content and favoring E_{oxi} and
433 E_T in the atmospheres containing SO_3. Therefore, the Hg-TPD analysis results were in
434 good consistence with the experimental results under different flue gas conditions.

435 3.6.2 XPS analysis

436 XPS analysis was conducted to investigate the existence forms of the surface
437 elements and the concentration ratios of each form in the corresponding element. Fig.
438 S4 showed the full-scale XPS spectra for the MnTi and FeMnTi catalyst samples. The

XPS spectra of element O for the MnTi catalyst after reacted in the different atmospheres involving SO_3, together with the fitting results, were shown in Fig. S5. The concentration ratios of different O species were calculated from the integral area of the corresponding fitting peaks, which were presented in Table 2. The fitting peaks at the binding energies of 529.7-529.9 eV and 532.2-532.3 eV were assigned to lattice oxygen (O_{latt}) and chemisorbed oxygen (O_{ad}), respectively (Zhang et al., 2020b). In addition, when SO_3 was contained in the reaction gas, an extra peak emerged at 530.9-531.0 eV in the spectra of the spent catalysts, which was distributed to oxygen of SO_4^{2-} ion (O_{sul}) (Yang et al., 2011). Meanwhile, the peak intensity and concentration ratios of O_{ad} decreased apparently on the catalysts spent in the presence of SO_3 compared to that spent in only N_2+O_2, while the ratio of O_{latt} showed ignorable changes. Thus, it demonstrated that the existence of SO_3 led to the generation of sulfate on the catalyst. And the formation of sulfate consumed the intrinsic O_{ad} of the catalyst which was one of the main active species for catalytic reaction. The formation of the persistent sulfate and the consumption of O_{ad} resulted jointly in the inhibitory effect of SO_3 on the Hg^0 removal efficiency. The ratio of O_{sul} after the reaction at 250 ℃ was lower than that after reacted in the same atmosphere at 150 ℃, indicating that the sulfate was partially decomposed at the higher temperature. And it explained the experimental results that the inhibition of SO_3 on E_T was gradually attenuated with the raise of the temperature. At the same temperature, the addition of H_2O led to a further increment of the O_{sul} ratio, while the ratio of O_{ad} was further lessened. This provided a clear interpretation for the greater inhibition on E_T caused by the introduction of H_2O into the SO_3-contained flue

461 gas.

462 The XPS curves of element Hg for the fresh and spent MnTi catalysts were shown
463 in Fig. S6. No peaks corresponding to Hg compounds were detected on the spectra of
464 the fresh catalyst. As the catalyst was spent in N_2+O_2 at 250 ℃, a fitting peak emerging
465 at 100.8 eV which stood for HgO was observed on the curve (Xu et al., 2016; Wu et al.,
466 2019), suggesting that HgO was generated on the catalyst surface after the reaction. By
467 contrast, upon the spectra of the catalysts spent in N_2+O_2+SO_3 and N_2+O_2+SO_3+H_2O
468 at 250 ℃, another fitting peak was obtained at 102.0-102.1 eV besides the peak of HgO,
469 which was assigned to $HgSO_4$ (Zhang et al., 2015, 2017c). Therefore, HgO and $HgSO_4$
470 were produced synchronously under these flue gas conditions. According to the integral
471 results of the fitting peaks presented in Table 3, the addition of H_2O into the reaction
472 gas made the ratio of $HgSO_4$ in the Hg compounds increase, which further indicated
473 that the coexistence of SO_3 and H_2O was conductive to the formation of $HgSO_4$. For
474 the catalysts after reacted in the presence of SO_3 at 150 ℃, the sole fitting peak of HgO
475 in the XPS spectra implied that $HgSO_4$ could be only generated at relatively higher
476 temperature. The peak intensity of HgO of the catalyst spent in N_2+O_2+SO_3+H_2O was
477 weaker than that of the catalyst spent in N_2+O_2+SO_3, which demonstrated the inhibition
478 of H_2O on Hg adsorption. There were no peaks corresponding to Hg^0 detected on the
479 spectra of all the catalyst samples, manifesting that the adsorption content of Hg^0 might
480 be lower than the detection limit of the XPS analysis referring to the Hg-TPD results.
481 Overall, the XPS results of Hg 4f showed good agreement with the Hg-TPD results.

482 Besides Hg, the element Mn in the catalysts and element Fe in FeMnTi might also

483 bond with the SO_4^{2-} ion, thereby bringing impacts on the catalytic efficiency. It could
484 be proven by the testing results of O 1s and Hg 4f after reaction at 150 ℃. That is,
485 sulfate was formed on the catalysts, but $HgSO_4$ was not detected, implying that the
486 combination between SO_4^{2-} and Mn or Fe had a high possibility. In order to verify this
487 conjecture, the speciation of element Mn and Fe on the spent catalysts was investigated
488 as well, and the catalyst samples after reacted at 250 ℃ were taken as the instance. The
489 analysis results of Mn 2p were shown in Fig. S7. The fitting peak appeared at 642.7-
490 642.9 eV and 641.2 eV in the spectra of MnTi and FeMnTi after spent in N_2+O_2
491 represented the species of Mn^{4+} and Mn^{3+}, respectively (Meng et al., 2019; Wang et al.,
492 2015). Mn^{4+} was demonstrated previously to be the active Mn species that would
493 participate in Hg^0 oxidation (Zhang et al., 2017a). After the catalysts were applied in
494 the SO_3-contained flue gas, a peak emerging at 644.0-644.2 eV was assigned to $MnSO_4$
495 (Yang et al., 2011). The calculated concentration ratios of Mn^{4+}, Mn^{3+} and $MnSO_4$ in
496 element Mn of the catalysts were listed in Table 4. $MnSO_4$ was formed on the catalysts
497 after reaction in the presence of SO_3 while the ratio of Mn^{4+} reduced obviously
498 compared to that after reacted in N_2+O_2, illustrating the catalysts were venenated by
499 SO_3. Combining with the analysis result of element O that O_{ad} was consumed during
500 the generation of sulfate as well, $MnSO_4$ was probably formed via reaction (3). That

501 $$Mn^{4+} + 2O^{2-} + SO_3 + O_{ad} \rightarrow MnSO_4 + O_2 \quad (3)$$

502 was Mn^{4+} and SO_3 together with O_{ad} occurred the reaction to form $MnSO_4$. O^{2-}
503 represented the lattice oxygen of MnO_2 which provided Mn^{4+}, and it incorporated into
504 $MnSO_4$ after the reaction. The injection of H_2O in the flue gas augmented the ratio of

505 $MnSO_4$ and further suppressed the ratio of Mn^{4+}, indicating that H_2O aggravated the
506 toxicity of SO_3 on the catalyst by accelerating the sulfation of the active species. The
507 result was similar to that of the analysis on O 1s, which reduced the catalytic efficiency.
508 The reaction process could be described with reaction (4) and (5), in which the

509 $$SO_3 + H_2O \rightarrow H_2SO_4 \quad (4)$$

510 $$Mn^{4+} + 2O^{2-} + H_2SO_4 + O_{ad} \rightarrow MnSO_4 + O_2 + H_2O \quad (5)$$

511 generated and condensed H_2SO_4 acted as the intermediate product. The ratio of the
512 produced $MnSO_4$ on FeMnTi was smaller than that on MnTi under the same atmosphere.
513 It decreased by 3.7% and 3.1% on FeMnTi compared to that on MnTi in the absence
514 and presence of H_2O, respectively, while the ratio of Mn^{4+} maintained the opposite
515 variation trend. The higher ratio of $MnSO_4$ on FeMnTi after spent in the presence of
516 H_2O than spent in the absence of H_2O also lent support to the experimental result that
517 H_2O impaired the Fe modification effect on E_T under the SO_3 condition.

518 As the results shown in Fig. S8, the element Fe on FeMnTi before and after reacted
519 in N_2+O_2 consisted of Fe^{2+}, octahedral coordinated Fe^{3+} and tetrahedral coordinated
520 Fe^{3+}, of which the fitting peaks appeared at 710.2 eV, 711.5 eV and 713.7-713.9 eV,
521 respectively (Yang et al., 2018a). The concentration ratios of the Fe species listed in
522 Table 5 reflected that there was little difference of the ratios of Fe^{2+} and Fe^{3+} between
523 the two catalysts, suggesting that Fe did not participate in the catalytic reaction in the
524 absence of SO_3. With the addition of SO_3, the fitting peak which represented $Fe_2(SO_4)_3$
525 emerged at 712.9 eV in the spectra of the spent catalysts additionally (Yang et al., 2011),
526 and the ratio of Fe^{3+} showed a descending trend. So $Fe_2(SO_4)_3$ was formed over FeMnTi

besides $MnSO_4$ in the presence of SO_3, and the process could be depicted by reaction (6). The further introduction of H_2O into the flue gas led to the extension of the ratio of

$$2Fe^{3+} + 3O^{2-} + 3SO_3 \rightarrow Fe_2(SO_4)_3 \quad (6)$$

the generated $Fe_2(SO_4)_3$, while the ratio of Fe^{3+} continued to decrease. Thus, H_2O facilitated the transformation of Fe^{3+} to $Fe_2(SO_4)_3$, of which the process was described by reaction (4) and (7). The ratio of Fe^{3+} decreased from 66.7% to 51.9% and 50% after

$$2Fe^{3+} + 3O^{2-} + 3H_2SO_4 \rightarrow Fe_2(SO_4)_3 + 3H_2O \quad (7)$$

the catalyst was spent in the presence of SO_3 and SO_3+H_2O, respectively. At the same time, the ratio of Mn^{4+} over FeMnTi was 7.5% and 4.9% larger than that over MnTi under the two working conditions respectively according to the results of Mn 2p, indicating that more Mn^{4+} was saved over FeMnTi in the formation of sulfate. The co-occurrence of the consumption of Fe^{3+} and the saving of Mn^{4+} demonstrated the intimate correlation between the two elements on the catalyst surface. That was Fe^{3+} acted as sacrificing site to combine with SO_4^{2-}, thereby expending the accessible SO_4^{2-} and making protection on Mn^{4+} from being poisoned to form $MnSO_4$ in a certain extent. The smaller ratio of $MnSO_4$ on FeMnTi than on MnTi after reaction in the same atmosphere could verify this inference. The Fe^{3+} consumed in the protection process, together with the active species of Mn^{4+} spent in the catalytic reaction of Hg^0 oxidation, could be replenished by gaseous O_2 in the flue gas to maintain the continuous operation of the catalyst. The Mn^{4+} that was saved by Fe^{3+} in the process would then participate in the Hg^0 oxidation through reaction (8) and (9). This was the predominant mechanism

$$Hg^0 + 2MnO_2 \rightarrow HgO + Mn_2O_3 \quad (8)$$

549 $$Hg^0 + SO_3 + 2MnO_2 \rightarrow HgSO_4 + Mn_2O_3 \quad (9)$$

550 for the generation of modification effect of Fe on the resistance of the MnTi catalyst to
551 SO_3 poisoning, which resulted in the higher E_T over FeMnTi than over MnTi in the
552 presence of SO_3.

553 ## 4. Conclusions

554 Effect of SO_3 on MnTi and Fe modified MnTi as the SCR catalysts for synergistic
555 Hg^0 removal was investigated systematically under different flue gas conditions in this
556 work. The results indicated that the increase of SO_3 concentration in the flue gas
557 produced irreversible inhibition on E_T of MnTi, which was mainly derived from the
558 reaction between SO_3 and surface Mn^{4+} and O_{ad} to generate $MnSO_4$, leading to the
559 catalyst deactivation. The further addition of H_2O into the flue gas would intensify the
560 suppression of SO_3 on E_T. Because higher temperature was favorable to the
561 decomposition of sulfate and could facilitate Hg^0 oxidation by SO_3, the inhibition of
562 SO_3 on E_T almost disappeared and even converted to promotion as the temperature
563 increased to 250 ℃ and above. Fe modification on MnTi improved the Hg^0 removal
564 performance of the catalyst in the presence of SO_3. The existence of Fe provided more
565 active sites and O_{ad} for the catalytic reaction, and it made protection on Mn^{4+} through
566 forming $Fe_2(SO_4)_3$, which was the major reason for enhancement on the resistance of
567 the catalyst to SO_3 poisoning. SO_3 showed no obvious influences on E_T of MnTi and
568 FeMnTi in simulated coal combustion flue gas at 250 ℃. The efficiencies were
569 inhibited by only 5.2% and 1.9%, respectively, and they could keep good stability over
570 a relatively long time. Therefore, the catalysts, especially FeMnTi, exhibited to be the

promising candidates as the low-temperature SCR catalyst for synergistic Hg^0 removal under actual flue gas condition.

In our future work, experiments under condition of SO_3 will be carried out with the coexistence of other individual flue gas components of HCl, NO and NH_3 to thoroughly explore the influence mechanisms of SO_3 on Hg^0 removal over the catalysts in coal burning flue gas. The results will be instructive for obtaining satisfactory Hg^0 removal performance of the catalysts under commercial operating conditions.

Acknowledgements

This research was supported financially by the National Natural Science Foundation of China (No. 52106169), the Natural Science Foundation of Shandong Province (No. ZR2021QE031), the China Postdoctoral Science Foundation (No. 2021M690097), the Foundation of State Key Laboratory of Coal Combustion (No. FSKLCCA2205), Taishan Scholars (No. ts201712003), the Postdoctoral Applied Research Project of Qingdao, and the Fundamental Research Funds of Shandong University (No. 2020GN008).

References

Benson, S.A., Laumb, J.D., Crocker, C.R., Pavlish, J.H., 2005. SCR catalyst performance in flue gases derived from subbituminous and lignite coals. Fuel Process. Technol. 86 (5), 577-613. https://doi.org/10.1016/j.fuproc.2004.07.004.

Fernández-Miranda, N., Lopez-Anton, M.A., Díaz-Somoano, M., Martínez-Tarazona, M.R., 2016. Mercury oxidation in catalysts used for selective reduction of NO_x (SCR) in oxy-fuel combustion. Chem. Eng. J. 285, 77-82. https://doi.org/10.1016/j.cej.2015.10.022.

He, P., Wu, J., Jiang, X., Pan, W., Ren, J., 2012. Effect of SO_3 on elemental mercury adsorption on a carbonaceous surface. Appl. Surf. Sci. 258 (22), 8853-8860. https://doi.org/10.1016/j.apsusc.2012.05.104.

Krishnakumar, B., Niksa, S., 2011. Predicting the impact of SO_3 on mercury removal by carbon sorbents. Proc. Combust. Inst. 33 (2), 2779-2785. https://doi.org/10.1016/j.proci.2010.06.057.

Li, C., Sriram, V., Liu, Z., Brewe, D., Lee, J.-Y., 2021. Sequentially prepared Mo-V-Based SCR catalyst for simultaneous Hg^0 oxidation and NO reduction. Appl. Catal. A: Gen. 614, 118032. https://doi.org/10.1016/j.apcata.2021.118032.

Li, H., Wu, C.-Y., Li, Y., Zhang, J., 2011. CeO_2-TiO_2 catalysts for catalytic oxidation of elemental mercury in low-rank coal combustion flue gas. Environ. Sci. Technol. 45 (17), 7394-7400. https://doi.org/10.1021/es2007808.

Li, H., Zhang, W., Wang, J., Yang, Z., Li, L., Shih, K., 2017. Coexistence of enhanced Hg^0 oxidation and induced Hg^{2+} reduction on CuO/TiO_2 catalyst in the presence of NO and NH_3. Chem. Eng. J. 330, 1248-1254. https://doi.org/10.1016/j.cej.2017.08.043.

Li, J., Chen, J., Ke, R., Luo, C., Hao, J., 2007. Effects of precursors on the surface Mn species and the activities for NO reduction over MnO_x/TiO_2 catalysts. Catal. Commun. 8 (12), 1896-1900. https://doi.org/10.1016/j.catcom.2007.03.007.

Lu, J., Zhou, Z., Zhang, H., Yang, Z., 2019. Influenced factors study and evaluation for SO_2/SO_3 conversion rate in SCR process. Fuel 245, 528-533. https://doi.org/10.1016/j.fuel.2019.02.077.

Masoomi, I., Kamata, H., Yukimura, A., Ohtsubo, K., Schmid, M.O., Scheffknecht, G., 2020. Investigation on the behavior of mercury across the flue gas treatment of coal combustion power plants using a lab-scale firing system. Fuel Process. Technol. 201, 106340. https://doi.org/10.1016/j.fuproc.2020.106340.

Meng, J., Duan, Y., Hu, P., Xu, Y., Geng, X., Yao, T., Ren, S., Wei, H., 2019. Simultaneous removal of elemental mercury and NO from simulated flue gas at low temperatures over Mn-V-W/TiO_2 catalysts. Energy Fuels 33 (9), 8896-8906. https://doi.org/10.1021/acs.energyfuels.9b01503.

Obrist, D., Agnan, Y., Jiskra, M., Olson, C.L., Colegrove, D.P., Hueber, J., Moore, C.W., Sonke, J.E., Helmig, D., 2017. Tundra uptake of atmospheric elemental mercury drives Arctic mercury pollution. Nature 547, 201-204. https://doi.org/10.1038/nature22997.

Presto, A.A., Granite, E.J., 2007. Impact of sulfur oxides on mercury capture by activated carbon. Environ. Sci. Technol. 41 (18), 6579-6584. https://doi.org/10.1021/es0708316.

Presto, A.A., Granite, E.J., Karash, A., 2007. Further investigation of the impact of sulfur oxides on mercury capture by activated carbon. Ind. Eng. Chem. Res. 46 (24), 8273-8276. https://doi.org/10.1021/ie071045c.

Rumayor, M., Díaz-Somoano, M., Lopez-Anton, M.A., Martínez-Tarazona, M.R., 2015a. Application of thermal desorption for the identification of mercury species in solids derived from coal utilization. Chemosphere 119, 459-465. https://doi.org/10.1016/j.chemosphere.2014.07.010.

Rumayor, M., Fernández-Miranda, N., Lopez-Anton, M.A., Díaz-Somoano, M., Martínez-Tarazona, M.R., 2015b. Application of mercury temperature programmed desorption (HgTPD) to ascertain mercury/char interactions. Fuel Process. Technol. 132, 9-14. https://doi.org/10.1016/j.fuproc.2014.12.032.

Rumayor, M., Gallego, J.R., Rodríguez-Valdés, E., Díaz-Somoano, M., 2017. An assessment of the environmental fate of mercury species in highly polluted brownfields by means of thermal desorption. J. Hazard. Mater. 325, 1-7. https://doi.org/10.1016/j.jhazmat.2016.11.068.

Sjostrom, S., Dillon, M., Donnelly, B., Bustard, J., Filippelli, G., Glesmann, R., Orscheln, T., Wahlert, S., Chang, R., O'Palko, A., 2009. Influence of SO_3 on mercury removal with activated carbon: Full-scale results. Fuel Process. Technol. 90 (11), 1419-1423.

https://doi.org/10.1016/j.fuproc.2009.08.019.
Tan, Y., Croiset, E., Douglas, M.A., Thambimuthu, K.V., 2006. Combustion characteristics of coal in a mixture of oxygen and recycled flue gas. Fuel 85 (4), 507-512. https://doi.org/10.1016/j.fuel.2005.08.010.
Uddin, M.A., Yamada, T., Ochiai, R., Sasaoka, E., Wu, S., 2008. Role of SO_2 for elemental mercury removal from coal combustion flue gas by activated carbon. Energy Fuels 22 (4), 2284-2289. https://doi.org/10.1021/ef800134t.
UNEP, 2019. Global mercury assessment 2018. UNEP Chemicals and Health Branch, Geneva, Switzerland. https://wedocs.unep.org/20.500.11822/27579.
Wang, Y., Shen, B., He, C., Yue, S., Wang, F., 2015. Simultaneous removal of NO and Hg^0 from flue gas over Mn-Ce/Ti-PILCs. Environ. Sci. Technol. 49 (15), 9355-9363. https://doi.org/10.1021/acs.est.5b01435.
Wu, X., Duan, Y., Li, N., Hu, P., Yao, T., Meng, J., Ren, S., Wei, H., 2019. Regenerable Ce-Mn/TiO_2 catalytic sorbent for mercury removal with high resistance to SO_2. Energy Fuels 33 (9), 8835-8842. https://doi.org/10.1021/acs.energyfuels.9b00978.
Wu, Z., Jiang, B., Liu, Y., Zhao, W., Guan, B., 2007. Experimental study on a low-temperature SCR catalyst based on MnO_x/TiO_2 prepared by sol-gel method. J. Hazard. Mater. 145 (3), 488-494. https://doi.org/10.1016/j.jhazmat.2006.11.045.
Xu, H., Zhang, H., Zhao, S., Huang, W., Qu, Z., Yan, N., 2016. Elemental mercury (Hg^0) removal over spinel $LiMn_2O_4$ from coal-fired flue gas. Chem. Eng. J. 299, 142-149. https://doi.org/10.1016/j.cej.2016.04.094.
Yang, J., Li, Q., Zhu, W., Qu, W., Li, M., Xu, Z., Yang, Z., Liu, H., Li, H., 2021. Recyclable chalcopyrite sorbent for mercury removal from coal combustion flue gas. Fuel 290, 120049. https://doi.org/10.1016/j.fuel.2020.120049.
Yang, J., Zhao, Y., Liang, S., Zhang, S., Ma, S., Li, H., Zhang, J., Zheng, C., 2018a. Magnetic iron-manganese binary oxide supported on carbon nanofiber ($Fe_{3-x}Mn_xO_4$/CNF) for efficient removal of Hg^0 from coal combustion flue gas. Chem. Eng. J. 334, 216-224. https://doi.org/10.1016/j.cej.2017.10.004.
Yang, S., Guo, Y., Yan, N., Qu, Z., Xie, J., Yang, C., Jia, J., 2011. Capture of gaseous elemental mercury from flue gas using a magnetic and sulfur poisoning resistant sorbent Mn/γ-Fe_2O_3 at lower temperatures. J. Hazard. Mater. 186 (1), 508-515. https://doi.org/10.1016/j.jhazmat.2010.11.034.
Yang, Z., Li, H., Qu, W., Zhang, M., Feng, Y., Zhao, J., Yang, J., Shih, K., 2019. Role of sulfur trioxide (SO_3) in gas-phase elemental mercury immobilization by mineral sulfide. Environ. Sci. Technol. 53 (6), 3250-3257. https://doi.org/10.1021/acs.est.8b07317.
Yang, Z., Zheng, C., Zhang, X., Zhou, H., Silva, A.A., Liu, C., Snyder, B., Wang, Y., Gao, X., 2018b. Challenge of SO_3 removal by wet electrostatic precipitator under simulated flue gas with high SO_3 concentration. Fuel 217, 597-604. https://doi.org/10.1016/j.fuel.2017.12.125.
Zhang, A., Zhang, Z., Lu, H., Liu, Z., Xiang, J., Zhou, C., Xing, W., Sun, L., 2015. Effect of promotion with Ru addition on the activity and SO_2 resistance of MnO_x-TiO_2 adsorbent for Hg^0 removal. Ind. Eng. Chem. Res. 54 (11), 2930-2939. https://doi.org/10.1021/acs.iecr.5b00211.
Zhang, H., Wang, T., Liu, J., Zhang, Y., Wang, J., Sun, B., Pan, W.-P., 2020a. Promotional effect of sulfur trioxide (SO_3) on elemental mercury removal over Cu/ZSM-5 catalyst. Appl. Surf. Sci. 511, 145604. https://doi.org/10.1016/j.apsusc.2020.145604.

Zhang, S., Díaz-Somoano, M., Zhao, Y., Yang, J., Zhang, J., 2019. Research on the mechanism of elemental mercury removal over Mn-based SCR catalysts by a developed Hg-TPD method. Energy Fuels 33 (3), 2467-2476. https://doi.org/10.1021/acs.energyfuels.8b04424.

Zhang, S., Zhang, Q., Zhao, Y., Yang, J., Xu, Y., Zhang, J., 2020b. Enhancement of CeO_2 modified commercial SCR catalyst for synergistic mercury removal from coal combustion flue gas. RSC Adv. 10 (42), 25325-25338. https://doi.org/10.1039/D0RA04350H.

Zhang, S., Zhao, Y., Wang, Z., Zhang, J., Wang, L., Zheng, C., 2017a. Integrated removal of NO and mercury from coal combustion flue gas using manganese oxides supported on TiO_2. J. Environ. Sci. 53 (3), 141-150. https://doi.org/10.1016/j.jes.2015.10.038.

Zhang, S., Zhao, Y., Yang, J., Zhang, J., Zheng, C., 2018. Fe-modified MnO_x/TiO_2 as the SCR catalyst for simultaneous removal of NO and mercury from coal combustion flue gas. Chem. Eng. J. 348, 618-629. https://doi.org/10.1016/j.cej.2018.05.037.

Zhang, S., Zhao, Y., Yang, J., Zhang, Y., Sun, P., Yu, X., Zhang, J., Zheng, C., 2017b. Simultaneous NO and mercury removal over MnO_x/TiO_2 catalyst in different atmospheres. Fuel Process. Technol. 166, 282-290. https://doi.org/10.1016/j.fuproc.2017.06.011.

Zhang, X., Li, Z., Wang, J., Tan, B., Cui, Y., He, G., 2017c. Reaction mechanism for the influence of SO_2 on Hg^0 adsorption and oxidation with $Ce_{0.1}$-Zr-MnO_2. Fuel 203, 308-315. https://doi.org/10.1016/j.fuel.2017.04.065.

Zhou, Y., Yang, J., Zhang, Y., Zhang, Y., Yu, X., Zhao, Y., Zhang, J., Zheng, C., 2019. Role of SO_3 in elemental mercury removal by magnetic biochar. Energy Fuels 33 (11), 11446-11453. https://doi.org/10.1021/acs.energyfuels.9b02567.

Zhuang, Y., Martin, C., Pavlish, J., Botha, F., 2011. Cobenefit of SO_3 reduction on mercury capture with activated carbon in coal flue gas. Fuel 90 (10), 2998-3006. https://doi.org/10.1016/j.fuel.2011.05.019.

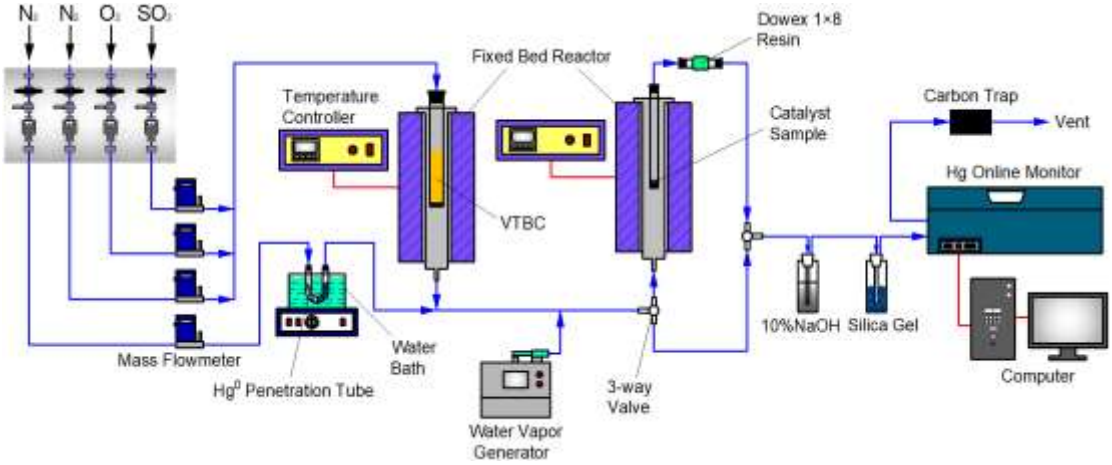

Fig. 1. Schematic diagram of the experimental system.

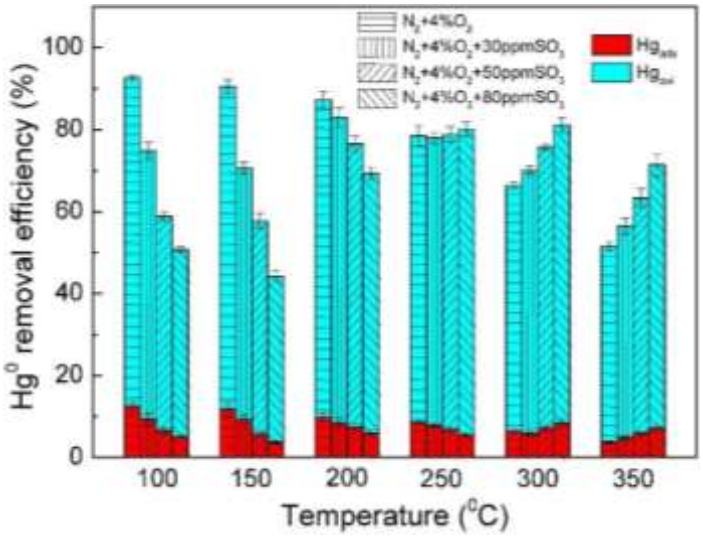

710

711 **Fig. 2.** Hg^0 adsorption and oxidation efficiencies of MnTi in the presence of different concentrations
712 of SO_3 at different temperatures.

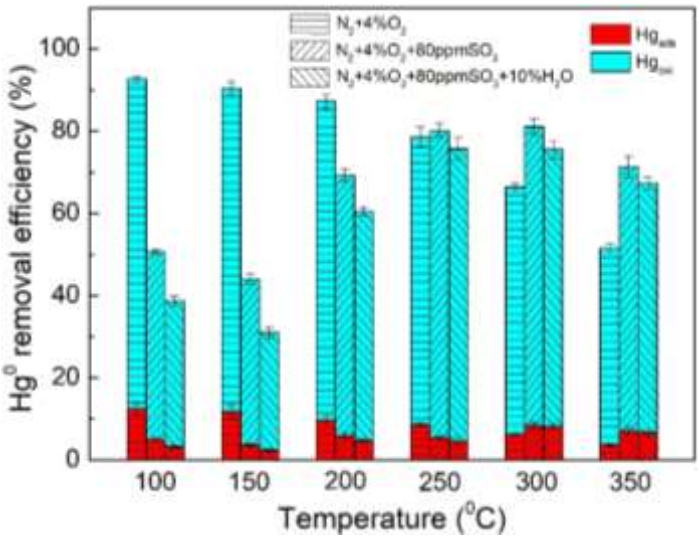

713

714 **Fig. 3.** Effect of SO_3 on Hg^0 adsorption and oxidation efficiencies of MnTi in the absence and
715 presence of H_2O at different temperatures.

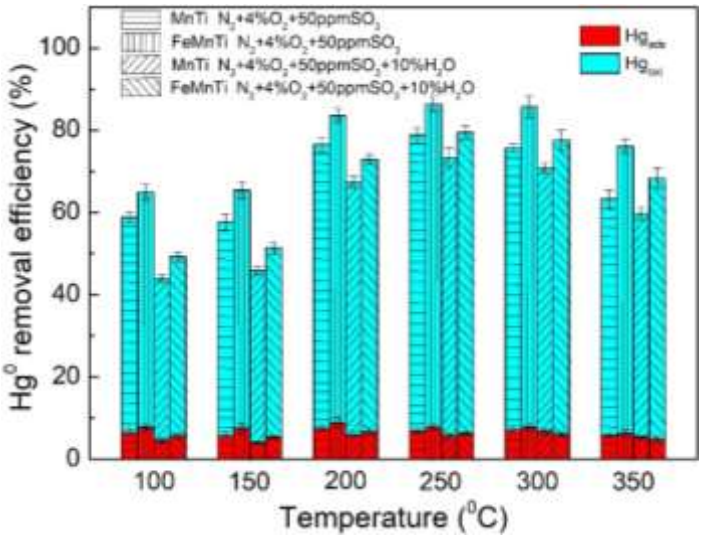

716

717 **Fig. 4.** Hg^0 adsorption and oxidation efficiencies of MnTi and FeMnTi under SO_3 condition in the
718 absence and presence of H_2O at different temperatures.

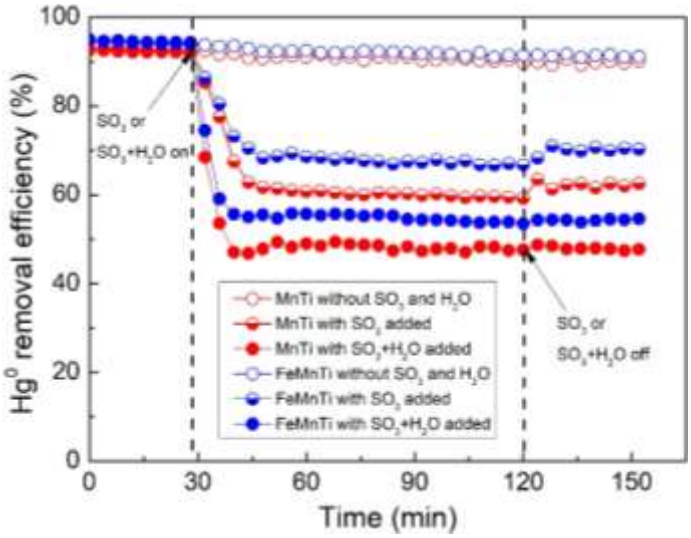

(a)

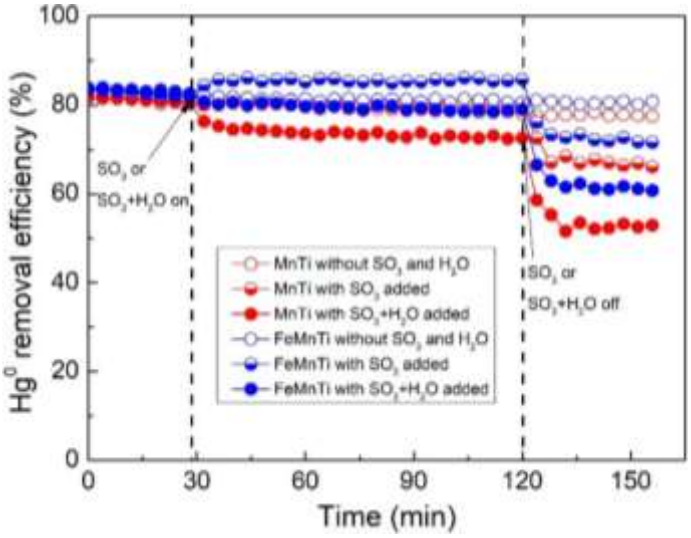

(b)

Fig. 5. Transient responses upon switching on and off 50 ppm SO_3 or 50 ppm SO_3 + 10% H_2O in N_2+4%O_2 at (a) 150 ℃ and (b) 250 ℃.

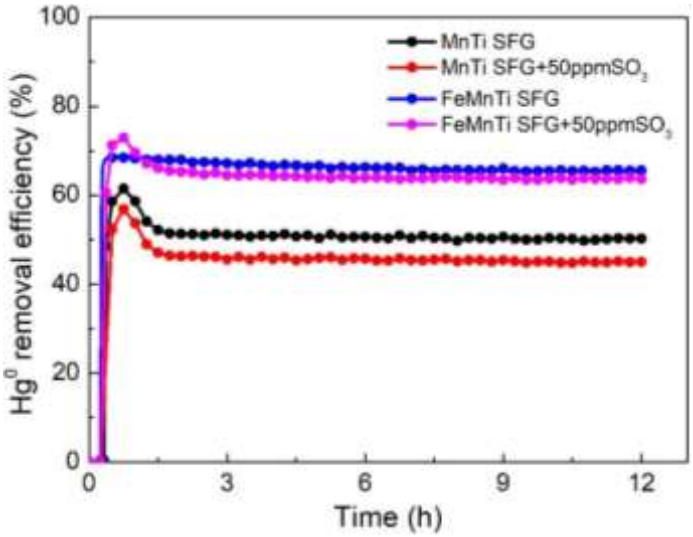

725

726 **Fig. 6.** Continuous measurement on Hg^0 removal efficiencies of MnTi and FeMnTi under simulated
727 coal-fired flue gas (SFG) without and with SO_3 contained in a 12 h period at 250 ℃. (SFG: N_2 +
728 4%O_2 + 12%CO_2+400 ppm SO_2 + 400 ppm NO + 400 ppm NH_3 + 10 ppm HCl + 10%H_2O)

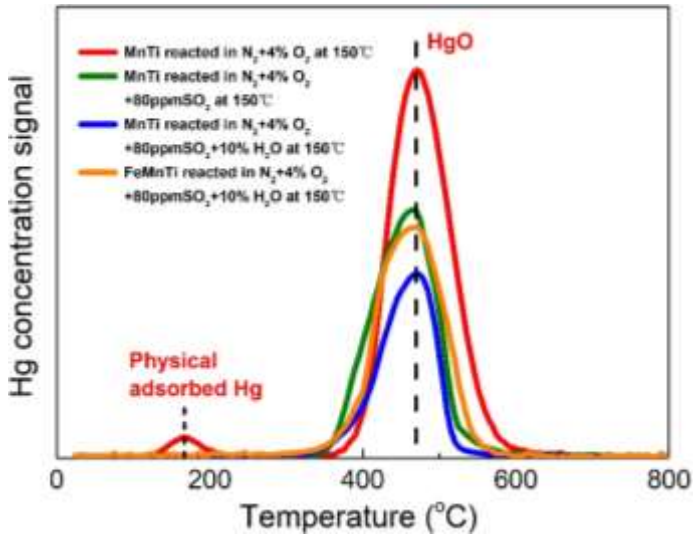

729
730 (a)

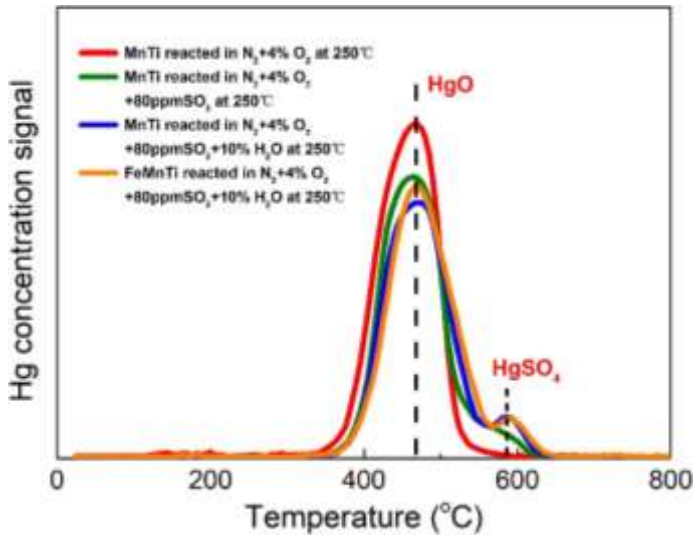

731
732 (b)

733 **Fig. 7.** Mercury thermal decomposition profiles of MnTi and FeMnTi after spent in different
734 reaction gases at (a) 150 ℃ and (b) 250 ℃.

735 **Table 1**

736 Hg^0 adsorption contents on MnTi and FeMnTi after reaction in the flue gas conditions involving
737 SO_3 determined by Hg-TPD (μg/g).

Catalyst	150 ℃	250 ℃
MnTi spent in N_2+4%O_2	1.858	1.553
MnTi spent in N_2+4%O_2+80ppmSO_3	1.235	1.360
MnTi spent in N_2+4%O_2+80ppmSO_3 +10%H_2O	0.806	1.329
FeMnTi spent in N_2+4%O_2+80ppmSO_3+10%H_2O	1.220	1.389

738 **Table 2**

739 The concentration ratios of different kinds of O atoms on MnTi after reaction in the flue gas
740 conditions involving SO_3 determined by XPS.

Catalyst	Ratio of O species (%)		
	O_{ad}	O_{sul}	O_{latt}
MnTi spent in N_2+4%O_2 at 250 ℃	37.8	/	62.2
MnTi spent in N_2+4%O_2+80ppmSO_3 at 150 ℃	19.8	20.9	59.3
MnTi spent in N_2+4%O_2+80ppmSO_3 at 250 ℃	24.5	15.6	59.9
MnTi spent in N_2+4%O_2+80ppmSO_3+10%H_2O at 150 ℃	17.6	26.2	56.2
MnTi spent in N_2+4%O_2+80ppmSO_3+10%H_2O at 250 ℃	21.8	20.1	58.1

Table 3

The concentration ratios of different kinds of Hg atoms on MnTi after reaction in the flue gas conditions involving SO_3 determined by XPS.

Catalyst	Ratio of Hg species (%)	
	HgO	$HgSO_4$
MnTi spent in N_2+4%O_2+80ppmSO_3 at 250 ℃	66.3	33.7
MnTi spent in N_2+4%O_2+80ppmSO_3+10%H_2O at 250 ℃	60.5	39.5

744 **Table 4**

745 The concentration ratios of different kinds of Mn atoms on MnTi and FeMnTi after reaction in the
746 flue gas conditions involving SO_3 determined by XPS.

Catalyst	Ratio of Mn species (%)		
	Mn^{4+}	Mn^{3+}	$MnSO_4$
MnTi spent in N_2+4%O_2 at 250 ℃	59.2	40.8	/
FeMnTi spent in N_2+4%O_2 at 250 ℃	63.4	36.6	/
MnTi spent in N_2+4%O_2+80ppmSO_3 at 250 ℃	48.3	34.9	16.8
FeMnTi spent in N_2+4%O_2+80ppmSO_3 at 250 ℃	55.8	31.1	13.1
MnTi spent in N_2+4%O_2+80ppmSO_3+10%H_2O at 250 ℃	44.6	34.4	21.0
FeMnTi spent in N_2+4%O_2+80ppmSO_3+10%H_2O at 250 ℃	49.5	32.6	17.9

747 **Table 5**

748 The concentration ratios of different kinds of Fe atoms on FeMnTi before and after reaction in the
749 flue gas conditions involving SO_3 determined by XPS.

Catalyst	Ratio of Fe species (%)		
	Fe^{3+}	Fe^{2+}	$Fe_2(SO_4)_3$
Fresh FeMnTi	66.7	33.3	/
FeMnTi spent in N_2+4%O_2 at 250 ℃	67.1	32.9	/
FeMnTi spent in N_2+4%O_2+80ppmSO_3 at 250 ℃	51.9	33.4	14.7
FeMnTi spent in N_2+4%O_2+80ppmSO_3+10%H_2O at 250 ℃	50.0	33.7	16.3